AFRL-RD-PS-
TP-2015-0010

SIMULTANEOUS PROCESSING OF VISIBLE AND LONG -WAVE INFRARED SATELLITE IMAGERY

Stacie Williams, et al.

19 October 2015

Technical Paper

AIR FORCE RESEARCH LABORATORY
Directed Energy Directorate
3550 Aberdeen Ave SE
AIR FORCE MATERIEL COMMAND
KIRTLAND AIR FORCE BASE, NM 87117-5776

NOTICE AND SIGNATURE PAGE

AFRL-RD-PS-TP-2015-0010 HAS BEEN REVIEWED AND IS APPROVED FOR PUBLICATION IN ACCORDANCE WITH ASSIGNED DISTRIBUTION STATEMENT.

// Thomas R. Swindle //	// Heather J. Anderson//
THOMAS R. SWINDLE, DR-II	HEATHER J. ANDERSON, Colonel, USAF
Program Manager	Chief, Space Electro-Optics Division

REPORT DOCUMENTATION PAGE

Form Approved
OMB No. 0704-0188

1. REPORT DATE *(DD-MM-YYYY)*	**2. REPORT TYPE**	**3. DATES COVERED** *(From - To)*
19-10-2015	Techncial Paper	01-10-2007 – 30-07-2015

4. TITLE AND SUBTITLE

Simultaneous Processing of Visible and Long-Wave Infrared Satellite Imagery

5a. CONTRACT NUMBER

In-House

5b. GRANT NUMBER

5c. PROGRAM ELEMENT NUMBER

6. AUTHOR(S)

Stacie Williams, *Michael Werth,*Brandoch Calef, *Daniel Thompson, **David Witte

5d. PROJECT NUMBER

5e. TASK NUMBER

EF002002

5f. WORK UNIT NUMBER

D01L

7. PERFORMING ORGANIZATION NAME(S) AND ADDRESS(ES)

Air Force Research Laboratory
3550 Aberdeen Avenue SE
Kirtland AFB, NM 87117-5776

*The Boeing Company
550 Lipoa Parkway
Kihei, HI 96753

**Pantera Consulting
1700Wells Drive NE
Albuquerque, NM 87112-4873

8. PERFORMING ORGANIZATION REPORT NUMBER

9. SPONSORING / MONITORING AGENCY NAME(S) AND ADDRESS(ES)

Air Force Research Laboratory
3550 Aberdeen Avenue SE
Kirtland AFB, NM 87117-5776

10. SPONSOR/MONITOR'S ACRONYM(S)

AFRL/RDSM

11. SPONSOR/MONITOR'S REPORT NUMBER(S)

AFRL-RD-PS-TP-2015-0010

12. DISTRIBUTION / AVAILABILITY STATEMENT

Approved for public release; distribution is unlimited. Government Purpose Rights.

13. SUPPLEMENTARY NOTES

14. ABSTRACT

One of the challenges of imaging satellites in the daytime is that the sun is generally behind the satellite from the observer's point of view. This means that much of the satellite structure can be in shadow at any given time. The Air Force Maui Optical and Supercomputing (AMOS) observatory's 3.6 meter telescope has the capability of recording data simultaneously in two bands of long-wave infrared (LWIR) as well as visible. This presents the possibility of performing joint processing of the infrared and visible imagery, which is appealing because the thermal imagery will not have any shadows. We describe exploitation strategies for this type of data, show the results of joint processing, and compare with single-band images.

15. SUBJECT TERMS

Multi-Frame Blind Deconvolution, Point Spread Function

16. SECURITY CLASSIFICATION OF:			**17. LIMITATION OF ABSTRACT**	**18. NUMBER OF PAGES**	**19a. NAME OF RESPONSIBLE PERSON**
a. REPORT	**b. ABSTRACT**	**c. THIS PAGE**			Ryan Swindle
Unclassified	Unclassified	Unclassified	SAR	14	**19b. TELEPHONE NUMBER** *(include area code)*

Standard Form 298 (Rev. 8-98)
Prescribed by ANSI Std. 239.18

This page intentionally left blank

TABLE OF CONTENTS

Section **Page**

LIST OF FIGURES

Simultaneous Processing of Visible and Long-Wave Infrared Satellite Imagery

Michael Werth, Brandoch Calef, Daniel Thompson
The Boeing Company

David Witte
Pantera

Stacie Williams
Directed Energy Directorate, Air Force Research Laboratory, Kirtland AFB, NM 87117

ABSTRACT

One of the challenges of imaging satellites in the daytime is that the sun is generally behind the satellite from the observer's point of view. This means that much of the satellite structure can be in shadow at any given time. The Air Force Maui Optical and Supercomputing (AMOS) observatory's 3.6 meter telescope has the capability of recording data simultaneously in two bands of long-wave infrared (LWIR) as well as visible. This presents the possibility of performing joint processing of the infrared and visible imagery, which is appealing because the thermal imagery will not have any shadows. We describe exploitation strategies for this type of data, show the results of joint processing, and compare with single-band images.

1.0 INTRODUCTION

The 3.6 meter Advanced Electro-Optical System (AEOS) telescope at the AMOS observatory is a satellite-tracking telescope that is capable of simultaneously recording data with sensors that are sensitive to visible and long-wave infrared (LWIR) wavelengths. Visible satellite images taken during daytime conditions are processed into high-resolution images with a variety of techniques [1,2], but satellite characteristics and pass geometry can still result in details that are difficult to see even if the resolved images have resolution that is close to diffraction limited. LWIR images suffer less from shadowing but also have much worse resolution than visible images. Combining information from both wavebands should allow for the creation of high-resolution images with details that are easier to observe. Furthermore, there's the possibility that fuzzy edge detection techniques could be used with LWIR images to create an object support constraint that would further improve the initial image processing results.

In section 2, the AEOS LWIR sensor and recent developments in LWIR data processing are described. Section 3 shows results from techniques that use LWIR images to improve the quality of well-resolved visible images, enhancing dark regions and reducing remaining blur. Section 4 shows results from using LWIR imagery as an object support constraint in blind deconvolution processing of visible imagery. Our conclusions are summarized in section 5.

2.0 AEOS LWIR SENSOR

The AEOS LWIR sensor is designed to provide imagery of targets in long wave infrared wavebands. A dichroic mirror splits the light beam onto two focal plane arrays so that data in two different infrared wavebands may be recorded simultaneously. Data analysts at the Maui High Performance Computing Center (MHPCC) use the images to perform luminosity and temperature measurements.

Recent updates to the LWIR system include automation of processing and optimization of processing algorithms. Images are now automatically transferred from data acquisition systems to data processing systems. Radiometric calibration star collections undergo automated data quality assessments. Good star data is used to calibrate luminosity measurements of the target. Temperature measurements, luminosity curves, and collection metadata are included in an automatically generated report that is then sent to interested parties. Fig. 1 shows a diagram describing how LWIR data is processed.

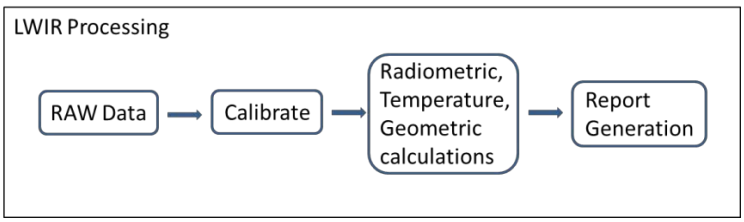

Fig.1. Flowchart of the LWIR processing

3.0 IMAGE DESHADOWING

Data was simultaneously recorded on the visible imaging sensor with an I-band filter and on the LWIR sensor during high elevation passes of the Fermi Gamma-ray Space Telescope, formerly the Gamma-ray Large Area Telescope (GLAST), and the Hubble Space Telescope (HST). The visible data was processed with a multi-frame blind deconvolution (MFBD) algorithm [1], successfully removing most of the atmospheric blur. A sample of the MFBD processed images and the calibrated LWIR images in the same field of view (FOV) are shown in Fig. 2.

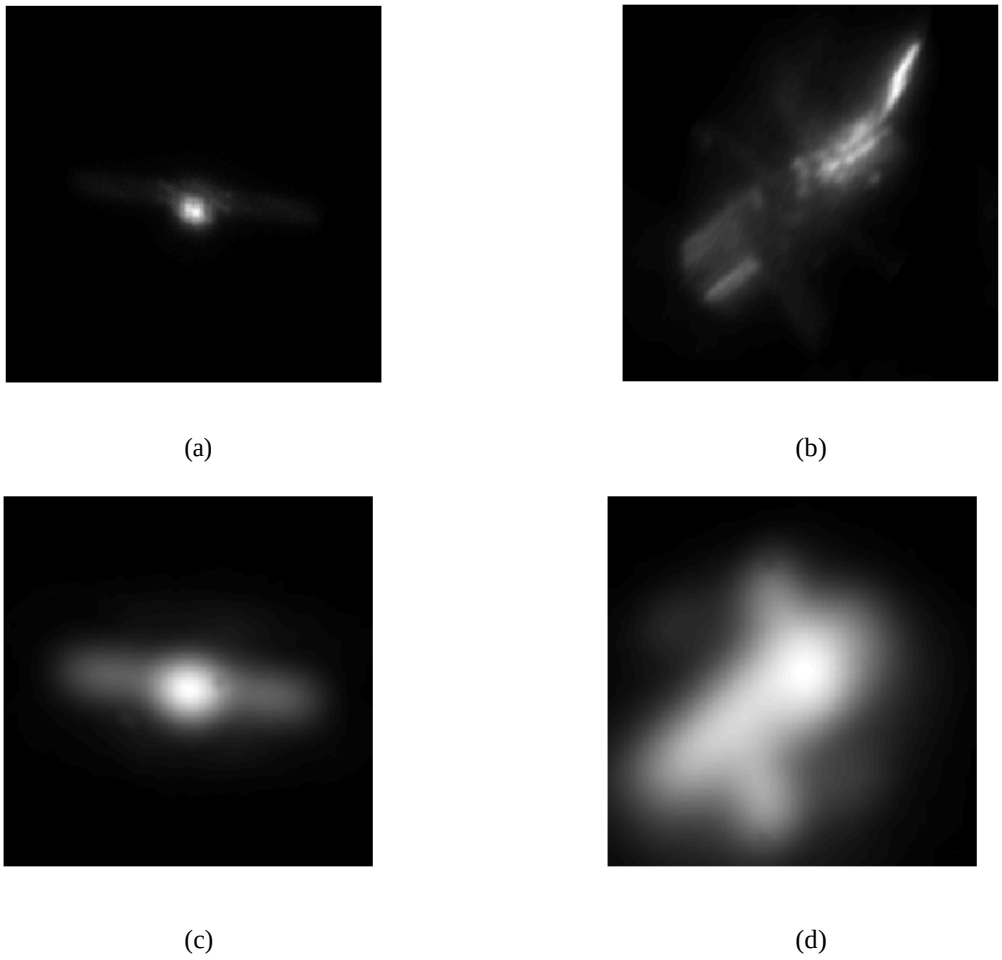

(a) (b)

(c) (d)

Fig. 2. (a) Visible GLAST data after MFBD processing, (b) visible HST data after MFBD processing, (c) LWIR GLAST and (d) LWIR HST data

The LWIR images are significantly blurrier than the MFBD-processed visible images, but they also do not suffer from shadowing effects that are present in the visible images. In particular, the LWIR images show the presence of

GLAST's solar panels and HST's solar panels and antennae, but these features in the visible imagery are difficult to see, especially HST's antennae. The dim features in the visible imagery can be brightened with a simple grayscale contrast enhancement, but this often results in the illumination of hazy artifacts that are left by the MFBD algorithm, as shown in Fig. 3.

Several image enhancement techniques have been developed, implemented, and tested on these passes. One of the most successful methods involves using the inverse of the LWIR image as a partially opaque mask that non-uniformly decreases the values of pixels in a combined visible-LWIR image. The visible and LWIR images are normalized to unity, and then the LWIR image is registered to the visible image. Each pixel of a combined image is calculated by taking the mean value of the LWIR and visible pixels at that location. This step is necessary in order to include features that are missing in the LWIR images, such as the hatch on HST. The result is inverted and shifted upward by a small scalar value in order to not have any zero-value elements in the final mask. The partial-opacity masks that result from this process are shown in Fig. 4.

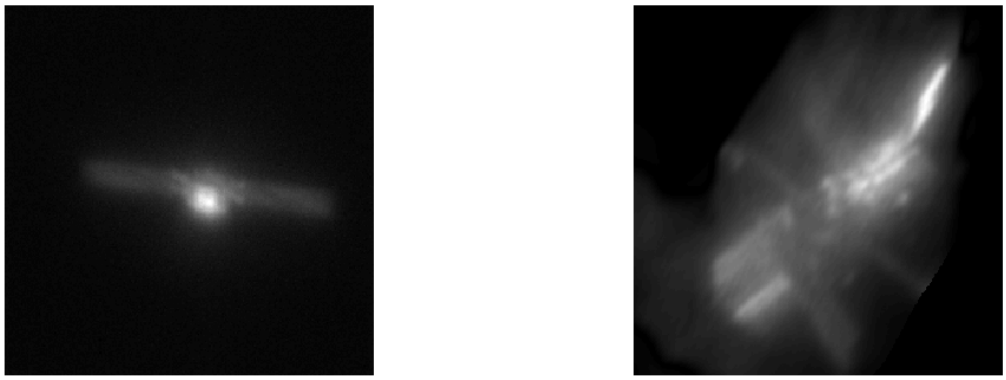

(a) (b)

Fig. 3. (a) Visible GLAST MFBD data and (b) visible HST MFBD data after contrast enhancement

(a) (b)

Fig. 4. (a) GLAST and (b) HST partial-opacity masks

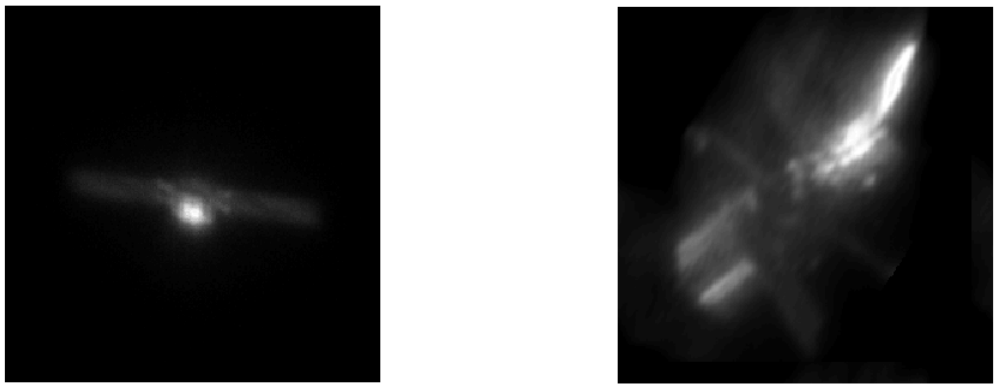

(a) (b)

Fig. 5. Visible (a) GLAST and (b) HST data after the full partial-opacity masking procedure has been applied

The MFBD-processed visible images shown in Fig. 2 are multiplied element-wise by the inversion masks in Fig. 4 to produce the enhanced images in Fig. 5. The panels and antennae are more visible in the resulting image, but there is still a small amount of haze obfuscating the panel edges. This is much more prevalent in the Hubble pass where the panels were already close to the background values. These results are promising; the dimmer features of the object become easier to see, and overall there is less haze than would appear due to a normal contrast adjustment.

The partial-opacity enhancement technique can be improved upon by using a Laplacian pyramid [3] to break down the images by frequency values before generating and applying the mask. Both the visible and LWIR images are broken down with a Laplacian pyramid, and then the low frequency components are enhanced with the partial opacity mask. The resulting images are then recombined to produce the images in Fig. 6. The dynamic range has been significantly reduced, allowing the dimmer aspects of the image to become visible but without the hazy artifacts present in Fig. 5. An additional contract enhancement, shown in Fig. 7, demonstrates that most of the haze around the object has been completely removed while leaving behind the desirable features.

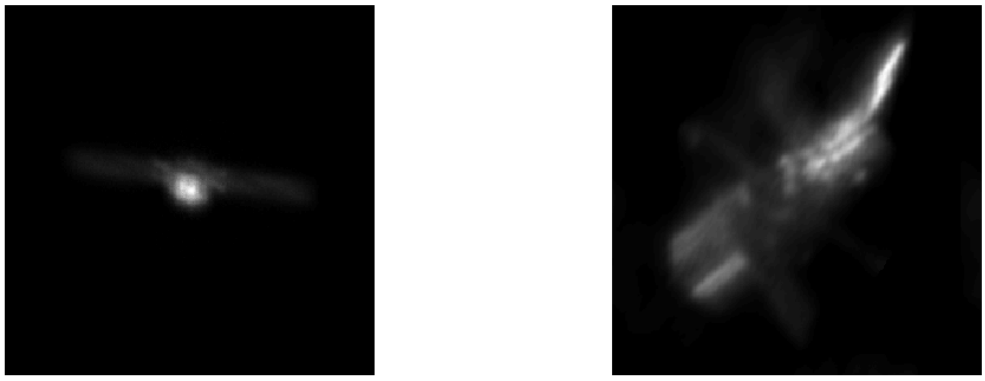

(a) (b)

Fig. 6. Visible (a) GLAST and (b) HST MFBD-processed images after Laplacian pyramid partial-opacity masking enhancement.

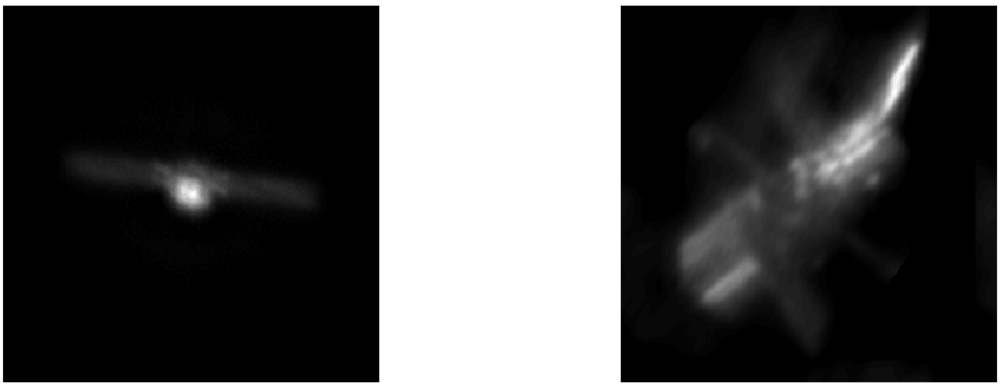

(a) (b)

Fig. 7. Visible (a) GLAST and (b) HST MFBD-processed images after Laplacian pyramid partial-opacity masking enhancement and additional gamma contrast enhancement.

4.0 MULTI-FRAME BLIND DECONVOLUTION WITH LWIR MASKING

Multi-frame blind deconvolution (MFBD) is a technique for deconvolving a pristine image from a blurring function. Our blurring function is a point spread function (PSF) dominated by atmospheric turbulence. Short-exposure images are used to estimate the PSF and produce an image with resolution approaching the diffraction limit of the optical system. Part of the MFBD process includes defining a region of the image for an initial estimate of the object, called the object support region. It can be difficult to algorithmically calculate a good object support region if the atmospheric blur is particularly strong. Images recorded in IR wavebands are less susceptible to turbulence effects and can produce a rough estimate of an object support constraint for use with MFBD processing.

Converting an LWIR image into an object support constraint requires converting the pixels that contain object information into a mask. The use of long wavelengths results in blurry images with edges that are difficult to detect with algorithms like Canny edge detection [4]. A pixel threshold filter can produce an acceptable mask, but with the risk of losing faint details. The Fast Multilevel Fuzzy Edge Detection (FMFED) algorithm [5] provides a good estimate of the object shape. This algorithm produces a conservative outline of the object, preserving faint details while suppressing noise information. An example of an LWIR image being converted into a mask with the FMFED algorithm is shown in Fig. 8. LWIR images are recorded in a much larger field of view than visible images, so the mask has to be expanded and cropped to the same dimensions as the visible imagery. The expanded mask and the expanded mask overlaid with an expanded LWIR image, for demonstrative purposes, are shown in Fig. 9.

(a) (b) (c)

Fig. 8. (a) Raw LWIR image of HST, (b) FMFED edges, and (c) FMFED mask

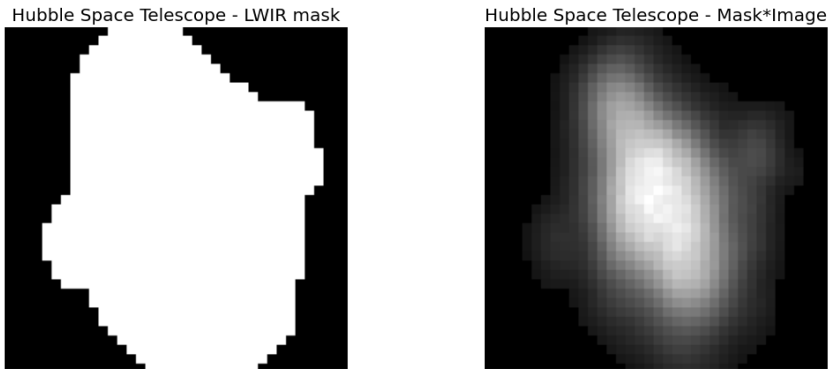

(a) (b)

Fig. 9**.** (a) The mask rescaled and cropped to same FOV as visible images and (b) the rescaled mask on top of the rescaled LWIR image

The MFBD algorithm was used to process the raw visible images with the mask from Fig. 9a provided as an object support constraint. For comparison, the MFBD algorithm was run a second time without an object support constraint. The results are shown in Fig. 10 and Fig. 11, but they are nearly identical to each other. A line spread function extraction technique [5] was chosen as a suitable method for assessing the relative quality of these images, but it indicated approximately no difference in quality regardless of whether the LWIR mask was provided. Image erosion and dilation algorithms were applied to the masks in order to tighten or loosen the constraint size, but there was still no improvement in the quality of the resultant images.

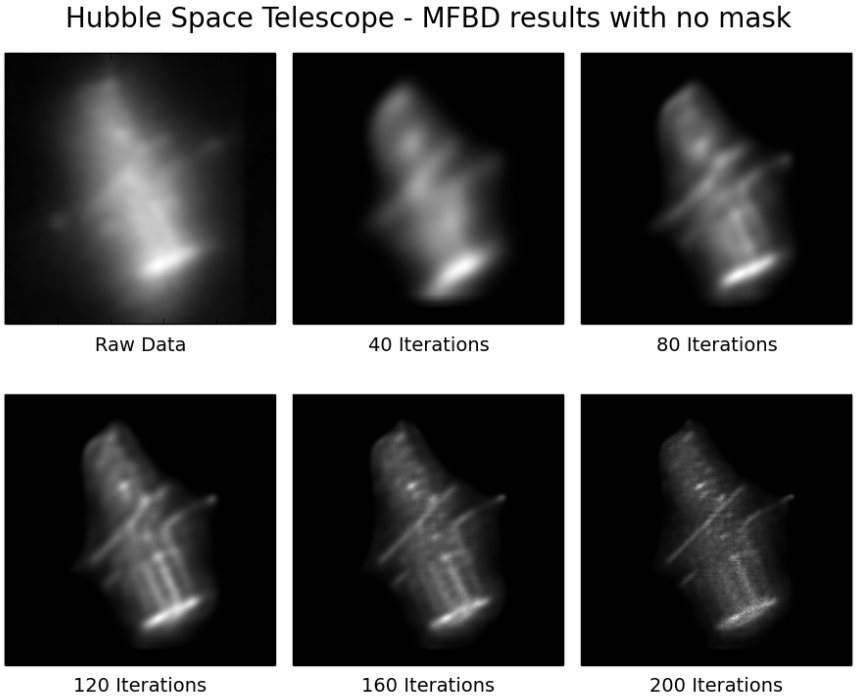

Fig. 10**.** MFBD results without a provided object support constraint.

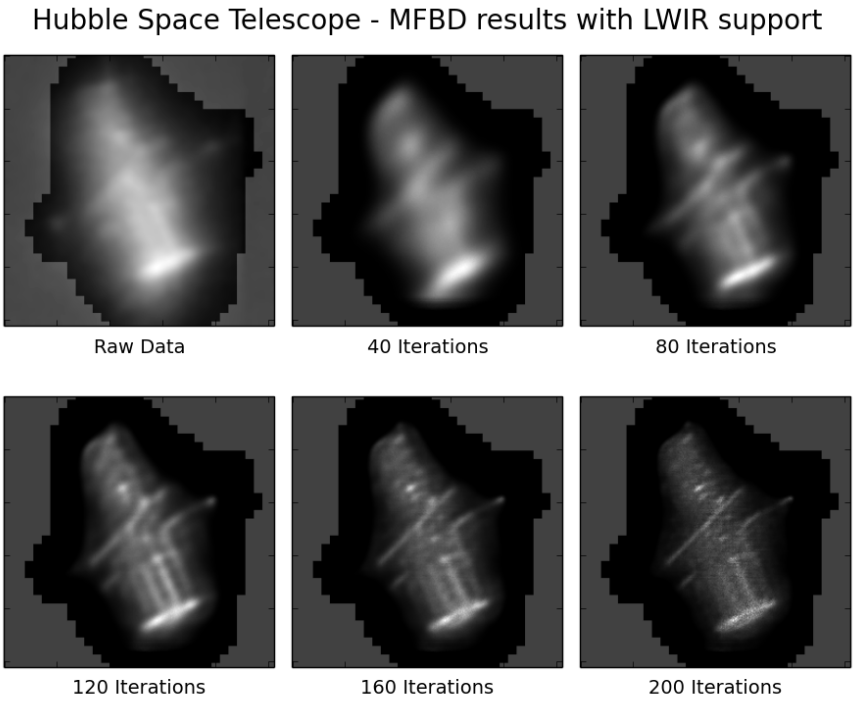

Fig. 11**.** MFBD results with an LWIR mask provided as the object support constraint and with the LWIR mask overlaid on top of the results for illustrative purposes

5.0 CONCLUSIONS

The AEOS telescope's LWIR sensor has been shown to provide image quality enhancements of simultaneously recorded visible images. The best results were obtained by using a Laplacian pyramid to split the LWIR and reconstructed visible images into several frequency ranges, using the LWIR images to create a partial-opacity mask that darkens the brightest parts of the visible satellite images in specific frequency ranges, and then recombining the visible images into a final enhanced image. We were successfully able to produce cleaner images with fewer shadows than the unenhanced MFBD results.

Attempts were made to use the LWIR images as an object support mask for MFBD processing, but no improvement was observed. It is possible that LWIR support in MFBD may only be beneficial when the atmospheric PSF has a much larger angular extent than the LWIR measurement. Future work will include an expanded survey of simultaneous passes for LWIR-mask MFBD processing in varied turbulence conditions.

6.0 REFERENCES

1 C. L. Matson, K. Borelli, S. Jefferies, C. C. Beckner, Jr., E. K. Hege, and M.L. Hart, *Fast and optimal multiframe blind deconvolution algorithm for high-resolution ground-based imaging of space objects*. Appl. Opt. 48, A75-A92 (2009).

2 A. W. Lohmann, G. Weigelt, and B. Wirnitzer, *Speckle masking in astronomy: triple correlation theory and applications*, Appl. Opt. 22, 4028–4037 (1983).

3 P. J. Burt and E. H. Adelson, *The Laplacian Pyramid as a Compact Image Code*. IEEE Transactions on Communications, vol.31, no.4, pp.532-540 (1983).

4 J. Canny, *A Computational Approach to Edge Detection*. IEEE Transactions on Pattern Analysis and Machine Intelligence, vol.PAMI-8, no.6, pp.679-698 (1986).

5 J. Wu, Z. Yin, Y. Xiong, *The Fast Multilevel Fuzzy Edge Detection of Blurry Images*, IEEE Signal Processing Letters, vol.14, no.5, pp.344-347 (2007).

6 M. Werth, J. Bos, B. Calef, S. Williams, and D. Thompson, *A new performance metric for hybrid adaptive optics systems*, IEEE Aerospace Conference (2014).

DISTRIBUTION LIST

DTIC/OCP
8725 John J. Kingman Rd, Suite 0944
Ft Belvoir, VA 22060-6218 1 cy

AFRL/RVIL
Kirtland AFB, NM 87117-5776 1 cy

Ryan Swindle, Project Officer
Official Record Copy
AFRL/RDSM 1 cy